



Article

Weak Fault Feature Extraction and Enhancement of Autonomous Underwater Vehicle Thrusters Based on Artificial Rabbits Optimization and Variational Mode Decomposition

Dacheng Yu, Mingjun Zhang, Feng Yao  and Jitao Li * 

College of Mechanical and Electrical Engineering, Harbin Engineering University, Harbin 150001, China; yudacheng@hrbeu.edu.cn (D.Y.); zhangmingjun@hrbeu.edu.cn (M.Z.); yaofeng@hrbeu.edu.cn (F.Y.)

* Correspondence: jitaoli@hrbeu.edu.cn

Abstract: Variational Mode Decomposition (VMD) has typically been used in weak fault feature extraction in recent years. The problem analyzed in this study is weak fault feature extraction and the enhancement of AUV thrusters based on Artificial Rabbits Optimization (ARO) and VMD. First, we introduce ARO to solve the problem of long-running times when using VMD for weak fault feature extraction. Then, we propose a VMD denoising method based on an improved ARO algorithm to address the issue of deteriorations in the fault feature extraction effect after introducing ARO. In this method, chaotic mapping and Gaussian mutation are used to improve ARO to optimize the parameters of VMD. This leads to a reduced running time and improved fault feature extraction performance. We then perform fault feature enhancement. Due to the unsatisfactory enhancement effect of traditional modified Bayes (MB) methods for weak fault features, we introduce energy operators to transform the fault signals into the energy domain for fault feature enhancement. Finally, we add differential processing to the signal to address the issue of certain fault feature values decreasing after introducing energy operators. In the end, the effectiveness of the proposed methods is verified via pool experiments on a “Beaver II” AUV prototype.

Keywords: Autonomous Underwater Vehicle; weak fault; Artificial Rabbits Optimization; fault feature extraction; fault feature enhancement; experiment study



Citation: Yu, D.; Zhang, M.; Yao, F.; Li, J. Weak Fault Feature Extraction and Enhancement of Autonomous Underwater Vehicle Thrusters Based on Artificial Rabbits Optimization and Variational Mode Decomposition. *J. Mar. Sci. Eng.* **2024**, *12*, 455. <https://doi.org/10.3390/jmse12030455>

Academic Editor: Marco Cococcioni

Received: 5 February 2024

Revised: 29 February 2024

Accepted: 4 March 2024

Published: 5 March 2024



Copyright: © 2024 by the authors. Licensee MDPI, Basel, Switzerland. This article is an open access article distributed under the terms and conditions of the Creative Commons Attribution (CC BY) license (<https://creativecommons.org/licenses/by/4.0/>).

1. Introduction

With the reduction in non-renewable resources on land, the development of marine resources is also gradually accelerating [1–3]. Marine development requires equipment. As marine development equipment, autonomous underwater vehicles (AUVs) play an important role in the development of marine resources due to their advantages of flexibility, large operation range, and so on [4–6]. AUVs operate in a complex marine environment without cables, and safety is one of the important focuses of AUV research and practical application [7–9]. The thruster is the most important power component in AUVs and is also one of the main sources of faults [10]. Studying the fault diagnosis technology used in the thruster has important research significance and practical value in relation to improving the safety of AUVs [11].

Most AUV thruster faults in the early stage are weak faults. If these faults are diagnosed and some safety measures, e.g., fault tolerance or self-rescue, are taken timely, most catastrophes can be avoided [11]. However, the premise of fault diagnosis is extracting the fault features. Due to the low signal-to-noise ratio of weak faults, it is difficult to separate the fault features from the noise interference. Therefore, the weak fault feature extraction of AUV thrusters has become a hot and challenging research topic in the field of weak fault diagnosis of AUV thrusters [12].

The process of thruster fault diagnosis mainly includes fault feature extraction, fault feature fusion, fault location, and fault severity identification [12].

This paper focuses on fault feature extraction for AUVs with weak thruster faults.

In terms of thruster fault feature extraction, the main methods include data-based methods, analytical-model-based methods, etc. [13,14]. Data-driven methods analyze the historical state information of AUVs to extract fault features, making them suitable for time-varying nonlinear systems. Therefore, they have become the mainstream approach to extracting fault features in AUV thrusters in recent years and have been widely used in the field of AUV fault diagnosis [15–17]. Typical methods include modified Bayes (MB) and Empirical Mode Decomposition (EMD) [18,19]. The advantages and shortcomings of the MB and EMD methods are summarized in Table 1.

Table 1. The advantages and shortcomings of MB and EMD.

Method	Advantage	Shortcoming
MB	Low complexity Insensitive to outliers in data Simple and easy to understand	Susceptible to noise Susceptible to data quality Mode mixing
EMD	Adaptive decomposition Analyzable nonlinear and non-stationary signal	Susceptible to noise Sensitive to outliers in data

Although both MB and EMD have some shortcomings, they are mostly effective in extracting fault features for strong faults (thrust losses greater than 10%) in AUV thrusters [18–20]. For example, in 2015, Zhang, Yin, Liu and Guo [18] fully utilized the excellent performance of MB in feature extraction to enhance the fault features of AUV thrusters. In 2019, Gong, Lv, Wang and Di [19] undertook the fault feature extraction of AUV thrusters using EMD. However, these approaches are not as effective in extracting fault features for weak faults (thrust losses less than 10%) [21]. The reason is that the thrust loss of weak faults is small, the fault feature is weak, the signal-to-noise ratio (SNR) is low, and the fault features are mixed with the frequency of interference signals.

In research on fault diagnosis theory, in 2014, Dragomiretskiy and Zosso [22] from the University of California, Los Angeles, proposed a new signal decomposition method called Variational Mode Decomposition (VMD). This method can adaptively determine the frequency range and amplitude of each mode, achieving the precise decomposition of the signal. This method is based on Wiener filtering, Hilbert transform, frequency mixing, and other methods. It solves a variational problem to determine the center frequency and bandwidth constraints. Then, it identifies the most effective components corresponding to each center frequency in the frequency domain to obtain the modes. This method has advantages in solving the problem of mode mixing between the fault feature signal and interference signal and has attracted attention in the field of fault diagnosis [23–25]. VMD has shown outstanding performance in extracting fault features (including weak fault features) for rotating machinery [26]. Yan and Jia [27] made full use of the excellent performance of VMD in feature extraction to realize the fault diagnosis of the bearing outer race. Wu et al. [28] proposed a method based on VMD cepstrum transformation, which applies VMD to the logarithmic spectrum of vibration signals to realize the fine diagnosis of composite faults of wind turbine gearboxes. In terms of AUV thruster fault feature extraction, in 2019, Feng, et al. [29] used VMD for the fault feature extraction of AUV thrusters and achieved good results.

VMD faces difficulties in selecting the parameters K (number of modes) and α (balance parameter) during its application. The selection of K and α directly affects the effectiveness of fault feature extraction. For different fault diagnosis objects, there is no uniform and appropriate method for selecting the parameters K and α . For the fault feature extraction of rotating machinery, in 2020, Zhao, et al. [30] proposed an adaptive parameter selection method based on permutation entropy, called MVMD. This method constructs a target formula based on the permutation entropy and iteratively selects the optimal parameters K and α . The method has a strong noise reduction capability and achieves better results in the fault diagnosis of rotating machinery such as bearings.

In 2022, we applied VMD for the first time to extract weak fault features of AUV thrusters [20]. In response to the unique underwater environment of AUVs, a modified MVMD method was proposed in [20] to select parameters K and α , which is based on negative entropy, and iteratively selects the optimal parameters K and α . The experimental results show that, for thruster weak faults, the method in reference [20] has good feature extraction effectiveness, especially in noise reduction. However, the problem is that the algorithm takes a long time (about 300 s). The reason for the long running time of the algorithm is the presence of multiple nested loops in the parameter optimization process, which leads to a slower convergence rate. Therefore, new intelligent optimization algorithms need to be investigated.

In 2022, Wang, et al. [31] proposed a new intelligent optimization algorithm, called Artificial Rabbits Optimization (ARO), which has the advantages of good convergence and a fast convergence rate.

We introduce the ARO algorithm to address the issue of the long runtime in the method proposed in reference [20] to optimize the parameters K and α in VMD based on the ARO algorithm. In the study, it was found that the ARO algorithm can effectively reduce the running time, but the convergence accuracy of the parameters K and α is low, resulting in the poor noise reduction effect of VMD, i.e., low SNR.

This paper proposes a noise reduction method (IARO-VMD) based on VMD with the improved ARO to address the above problems. This method utilizes chaotic mapping and Gaussian mutation to improve the ARO algorithm for optimizing parameters K and α in VMD. The purpose is to reduce the running time of the VMD-based noise reduction method proposed in reference [20] and obtain better convergence accuracy for parameters K and α , thereby improving the noise reduction effect. Comparative experiments are conducted to validate the proposed method.

The main focus of the above fault feature extraction approach is noise reduction. Afterward, fault feature enhancement needs to be performed. When we apply the classic fault feature enhancement method, the MB method, to enhance signals such as surge velocity signal and yaw angle signal, we encounter the following issue: for weak faults, although the MB method can enhance the fault feature, the effect of fault feature enhancement is not satisfactory. Therefore, further enhancement of fault features is needed to provide larger fault feature values for subsequent fault severity identification.

This paper proposes a weak fault feature enhancement method (EO-MB) based on the energy operator and MB to address the above problems. This method realizes the further enhancement of the weak fault features by converting and processing the fault feature signals in the time and energy domains. Corresponding improvements have been proposed to deal with the new problems caused by the introduction of the energy operator. Finally, a comparative experiment has been conducted to validate the proposed method.

In summary, this study makes the following contributions:

- (1) In this paper, we propose a noise reduction method called IARO-VMD, which is based on the improved ARO and VMD. This method combines ARO and VMD for the first time to extract weak fault features of AUV thrusters and reduce the running time. To further enhance the performance of the ARO method in extracting weak fault features of AUV thrusters, we employ chaotic mapping and Gaussian variational methods;
- (2) In this paper, we propose a method for enhancing weak fault features by combining the energy operator and MB. In this method, we first apply the energy operator to process the fault feature signals and transform them into the energy domain, thereby increasing the significance of the fault feature. Then, MB is used to analyze and model the signals in the energy domain more accurately, further enhancing the weak fault feature. Finally, we propose appropriate improvement methods to solve the new problem introduced by the energy operator.

The rest of the paper is organized as follows: In Section 2, the proposed IARO-VMD is illustrated. In Section 3, the proposed EO-MB is illustrated. In Section 4, the experimental validation of these two methods is conducted. Finally, conclusions are drawn in Section 5.

2. The IARO-VMD Method

We used the ARO algorithm to solve the problem of the long-running time required by the noise reduction method for AUV thruster fault signals, which is based on the VMD mentioned in reference [20]. However, it was found that although the ARO algorithm can effectively reduce the running time, the noise reduction effect is poor. Therefore, to solve this problem, an improved ARO optimization algorithm based on chaotic mapping and Gaussian variation is proposed in this section.

In this section, firstly, the reason for the long-running time when de-noising AUV thruster fault signals based on VMD is analyzed. Next, the problems that arise after introducing the ARO algorithm to solve the issue of the long-running time in VMD are analyzed, as are the reasons behind these problems. Finally, the improvement of the IARO-VMD method is outlined.

2.1. The Reason for the Long Running Time When De-Noising AUV Thruster Fault Signals Based on VMD

In the process of designing the optimization algorithm for noise reduction in AUV thruster fault signals based on VMD, three nested loops are used to achieve the required accuracy. The first loop is for the parameter α value, the second loop is for the parameter K value, and the third loop is for parameter K optimization. To ensure accuracy, the range of values for K and α is large. However, the large parameter range and the excessive number of loop iterations result in a long-running time when using the VMD algorithm to de-noise AUV thruster fault signals.

2.2. Analyzing the Problems That Exist and Their Reasons after Introducing the ARO Algorithm to Address the Issue of Long Running Time in the VMD Method

In 2022, Wang et al. [31] proposed a new intelligent optimization algorithm called ARO. This algorithm simulates the strategies of rabbits in the process of searching for food by continuously adjusting the search direction and search distance to find the optimal solution. It has the advantages of good convergence and fast convergence speed. It has been successfully applied in the field of rotating machinery fault diagnosis [32,33].

To address the problem of long runtime, we introduce the ARO algorithm, building up the method in reference [20].

When using the ARO algorithm to optimize VMD parameters and then using VMD for noise reduction, we found the following issues:

The above method can effectively reduce the running time of the algorithm (the running time is reduced by about 90%), but the noise reduction effect becomes worse.

The reasons are as follows:

- (1) The ARO method initializes the rabbit population using uniformly distributed random numbers, which lack randomness and traversal, leading to a tendency to fall into local optimal solutions;
- (2) In the later stage of iteration, there is no mechanism to escape from local optimal solutions, making it difficult to obtain the global optimal solution. When using the traditional ARO method to calculate fitness and update the position, each rabbit tends to update its position with another randomly selected rabbit in the population. This method uses random numbers that follow a standard normal distribution to increase perturbation as a way to enhance global search capabilities and avoid local optima. However, in the later stages of iteration, all search individuals cluster in a smaller region, and this setting precludes effective escape from local optima.

2.3. Improvements of the Proposed Method

This subsection describes improvements to the traditional ARO method. The flowchart of the VMD noise reduction method based on the traditional ARO is shown in Figure 1a, and the flowchart of the VMD noise reduction method based on the improved ARO method is shown in Figure 1b.

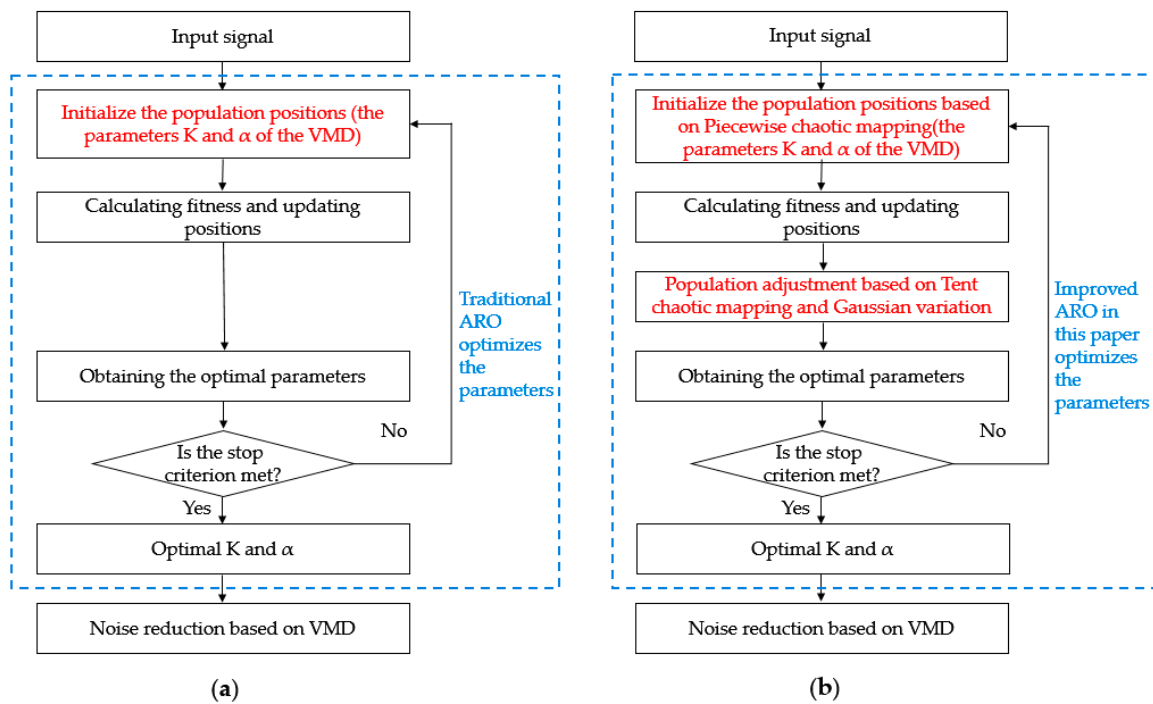


Figure 1. Comparison of the flowcharts of two methods: (a) The flowchart of the VMD noise reduction method is based on the traditional ARO. (b) The flowchart of the VMD noise reduction method is based on the improved ARO method.

Combining Figure 1a,b, we can derive the improved ARO method, the main concept of which is reflected in the following two points.

Improvement (1): Improve the method of initializing population positions.

The method for the initialization of population positions under the traditional ARO method is shown in Figure 1a. This method is generated by a uniform distribution random number generator, which lacks randomness and quickly falls into the local extremum.

The improved method of initializing population positions is shown in Figure 1b. In this method, a Piecewise chaotic map is used to initialize the population positions. Piecewise chaotic mapping can generate populations with greater randomness and diversity, thereby greatly reducing the probability of falling into local extremes.

The purpose of this paper is to address the time consumption of the VMD denoising method in reference [20] by improving the global search capability and convergence rate. Piecewise chaotic maps have the advantages of strong randomness and high diversity, which can enhance the global search capability and accelerate the convergence rate. This method has been successfully applied in the field of optimization [34,35]. Therefore, Piecewise chaotic maps are introduced into the initialization population in this study.

There are various types of chaotic maps, such as the tent map and the logistic map. The reason for choosing Piecewise chaotic maps in this study is because they are simple and easy to implement, have a fast computation speed, adjustable parameters, and a wide scope of application.

Improvement (2): Add a mechanism to escape local optimal solutions in the later stages of iteration.

From Figure 1a,b, it can be seen that the improved ARO method described in this paper adds an additional step after the “Calculate Fitness and Update Positions” step, differentiating it from traditional methods. This step is called “Population Adjustment based on Tent Chaotic Mapping and Gaussian Mutation”. The starting points for adding this step are as follows:

After calculating the fitness and updating the position, this study first performs population adjustment based on Tent chaos mapping and Gaussian mutation. This solves

the problem of determining the local optimal solutions in the later stages of iteration. Finally, this study updates and finds the current best solution.

Gaussian variation shows a small probability of moving the rabbit away from its current location, thereby increasing the likelihood of escaping from local optima. Tent chaos mapping can update the rabbit's position to a region far away from its current location, thereby avoiding repeated trapping in the same area and increasing the chance of escaping from local optima.

2.4. Implementation of the Proposed Method

Combined with Figure 1b, the specific implementation process of the proposed IARO-VMD method is explained. In this subsection, the improvements of the proposed method are highlighted, and the same steps as in the traditional method are briefly explained.

(1) Initialize the rabbit population positions based on Piecewise chaotic mapping

This step is an improvement offered by this study and is described in detail below.

The parameters K and α of the VMD are initialized by Piecewise chaotic mapping to generate an initial solution covering the entire search space.

The formula of the Piecewise chaotic map is as follows [36]:

$$x(t+1) = \begin{cases} \frac{x(t)}{p}, & 0 \leq x(t) < p \\ \frac{x(t)-p}{0.5-p}, & p \leq x(t) < 0.5 \\ \frac{1-p-x(t)}{0.5-p}, & 0.5 \leq x(t) < 1-p \\ \frac{1-x(t)}{p}, & 1-p \leq x(t) < 1 \end{cases} \quad (1)$$

where $0 < p < 0.5$ and $p = 0.4$ is established; $x(t)$ denotes the iteration value, and $x(1)$ is a random value.

(2) Calculating fitness and updating positions

This step contains the same processes as the traditional ARO [31] and is briefly outlined below.

The exploration and exploitation processes are performed, the fitness is calculated, and the position is updated. The specific content is the same as in the ARO method and will not be repeated here.

(3) Population adjustment based on Tent chaotic mapping and Gaussian variation

This step contains an improvement offered by this study and is described in detail below.

Let f_i be the fitness function value of the i -th rabbits and f_a be the average of the fitness function values of the population. The position is determined and updated in the following way:

- (a) If $f_i < f_a$, indicating the occurrence of "convergence", Gaussian mutation is performed. If the fitness function value of the new position is lower than the old position, the position is replaced.
- (b) If $f_i \geq f_a$, indicating the occurrence of "divergence", Tent chaotic mapping is performed. If the fitness function value of the new position is lower than the old position, the position is replaced.

Gaussian mutation is intended to add a random vector obeying a Gaussian distribution to the state of the original individual. Gaussian mutation is defined as follows:

$$G = X \times [1 + \sigma N(0, 1)] \quad (2)$$

where X denotes the original position of the rabbit, $\sigma N(0, 1)$ denotes a random number that follows a Gaussian distribution with mean 0 and variance 1, and G denotes the mutated position of the rabbit.

The formula for the Tent chaotic mapping is [37]:

$$x(t+1) = \begin{cases} \frac{x(t)}{p}, & x < p \\ \frac{1-x(t)}{1-p}, & p < x \leq 1 \end{cases} \quad (3)$$

where $x(t)$ denotes the value of the t -th iteration, and p takes on a random value in the range of $(0, 1)$.

(4) Obtaining the optimal parameters

This step is the same as that in the traditional ARO [31], and its process is briefly outlined below.

Via iteration and comparison, the optimal parameters K and α of the VMD are obtained.

(5) Noise reduction based on VMD

Based on the optimization parameters obtained in step (4), the signal is decomposed by VMD. This step is the same as that in the VMD-based noise reduction method in reference [20] and will not be repeated.

After the VMD decomposition, the modes with the highest noise content are removed, and the remaining modes are reconstructed as denoise signals.

3. The EO-MB Method

The focus of fault feature extraction described in Section 2 is on noise reduction. After that, fault feature enhancement is needed. The classical method for fault feature enhancement is MB [18,21]. For strong AUV thruster faults with a large degree of thrust loss, the fault feature enhancement of the MB method is very effective and can generally satisfy the requirements of subsequent fault severity identification. However, for weak AUV thruster faults, the fault feature enhancement effect of the MB method is not satisfactory, and the enhanced fault feature values are still relatively small. Therefore, further enhancement of fault features is required to provide larger fault feature values for the subsequent weak fault severity identification. In this section, a weak fault feature enhancement method based on energy operators and MB is proposed.

In this section, the reasons why the MB method has an unsatisfactory enhancement effect on weak fault features are first briefly analyzed. Then, we analyze the problems that arise after the introduction of energy operators and their causes. Finally, the steps for the improvement and implementation of the proposed EO-MB method are explained.

3.1. Problems of MB

The reasons for the unsatisfactory enhancement effect of the MB method on weak fault features are as follows.

When weak faults occur, the changes in the signal caused by the faults are very small and show little difference from noise and other interferences. Although the method in Section 2 reduces the influence of noise and other interferences, it still does not significantly enhance the weak fault features obtained based on the MB method.

3.2. Introduction of Energy Operator

(1) Introducing energy operator

In recent years, energy operators have attracted attention and found applications in the weak fault diagnosis of rotating machinery [38,39]. Energy operators convert signals from the time domain to the energy domain through nonlinear transformations. They are sensitive to signal changes, enhance the transient characteristics of signals, and quickly track signal changes. We introduce energy operators into the MB method to solve the problem of the unsatisfactory enhancement effect of weak fault features in AUV thrusters using the MB method.

(2) Problems arising after introducing the energy operator

Here, we introduce an energy operator into the MB method. After fault feature extraction and before fault feature enhancement using the MB method, signal processing

based on the energy operator is performed to transform the signal from the time domain to the energy domain. This enhances the transient characteristics of the signal. The aim is to further improve the weak fault feature enhancement effect of the MB method.

After introducing the energy operator, the problem discovered is that, for velocity signals, the introduction of energy operators can improve the enhancement of weak fault features using the MB method. However, for the yaw angle signal, lateral thruster control signal, and main thruster control signal, the introduction of energy operators reduces the enhancement effect.

(3) Analysis of the causes of the above problems

The energy operator can reflect instantaneous changes in energy. However, after a fault occurs, the changes in the yaw angle signals, as well as the main thruster control voltage signals and lateral thruster control voltage signals, are relatively gradual and small in magnitude. This makes it difficult for the energy operator to effectively enhance the transient characteristics at the moment of fault occurrence, ultimately leading to a weak effect of the MB method on the weak fault feature enhancement of signals such as the yaw angle signal.

(4) Ideas for improved methods in this study

Based on the above analysis, to increase the variation of the yaw angle signal, lateral thruster control signal, and main thruster control signal, here, after a weak fault occurs, these signals are firstly differentiated, and then signal enhancement based on an energy operator is carried out.

3.3. Methods in This Study

(1) The process and improvement of the proposed method

A flowchart of the traditional MB method is shown in Figure 2a, and a flowchart of the EO-MB method used in this study is shown in Figure 2b.

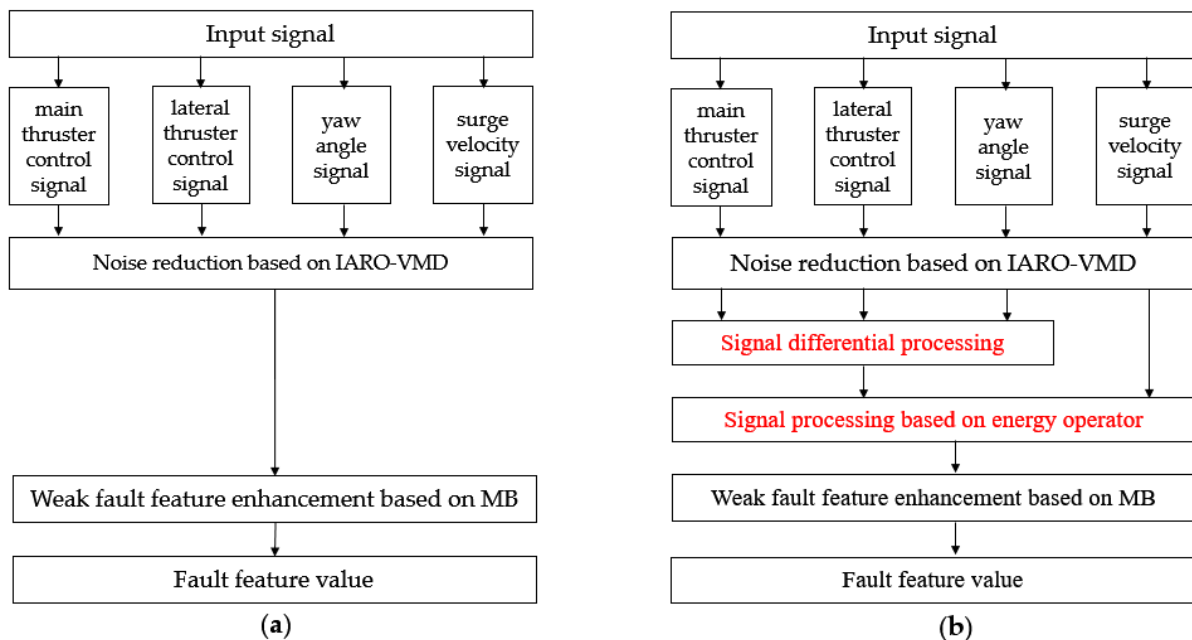


Figure 2. Comparison of the flowchart of two methods: (a) flowchart of the traditional MB method and (b) flowchart of the EO-MB method in this study.

In the combination of Figure 2a,b, the potential improvements of the proposed weak fault feature enhancement method are illustrated, as reflected in the following two points.

Improvement (1): Introducing energy operator

The traditional method uses MB to directly enhance the weak fault features of all de-noised input signals, as shown in Figure 2a.

In this study, after the “noise reduction using improved ARO-based VMD” step, an additional step of “signal processing using energy operator” is introduced, as shown in Figure 2b.

Improvement (2): Adding a step of “signal differentiation processing”

To solve the problem of the poor performance of the yaw angle, lateral thruster control, and main thruster control signals, a “signal differentiation processing” step is added before the “energy operator signal processing” for these signals, as shown in Figure 2b.

(2) Specific implementation steps of the proposed method

In Figure 2b, the specific implementation process of this method is explained. This subsection focuses on the improvements of this method while briefly explaining the steps that are consistent with those in the traditional MB method.

(a) Noise reduction based on IARO-VMD

This step employs the noise reduction method proposed in Section 2. Here, we will briefly describe its process.

The surge velocity, main thruster control voltage, lateral thruster control voltage, and yaw angle signals are de-noised by the IARO-VMD method, a VMD noise reduction method based on the improved ARO proposed in Section 2.

(b) Signal differential processing

This step is one of the improvements of this study and is described in detail as follows.

The yaw angle signal, lateral thruster control signal, and main thruster control signal are differentiated to obtain their respective differential signals. The differential equations are as follows:

$$\Delta x(t) = x(t) - x(t - 1) \tag{4}$$

where Δx denotes a differential signal, and $x(t)$ denotes the denoised value at the t -th moment.

(c) Signal processing based on energy operator

This step is one of the improvements of this study and is described in detail as follows.

The energy operator expression is used to convert the surge velocity signal, the yaw angle differential signal, the lateral thruster control differential signal, and the main thruster control differential signal to the energy domain, respectively. This results in their corresponding energy operator signals.

The energy operator signals for each signal can be calculated by the following expressions [39]:

$$T[sv(n)] = [sv(n)]^2 - sv(n + 1) \cdot sv(n - 1) \tag{5}$$

$$T[ya(n)] = [ya(n)]^2 - ya(n + 1) \cdot ya(n - 1) \tag{6}$$

$$T[ltn(n)] = [ltn(n)]^2 - ltn(n + 1) \cdot ltn(n - 1) \tag{7}$$

$$T[mt(n)] = [mt(n)]^2 - mt(n + 1) \cdot mt(n - 1) \tag{8}$$

where $sv(n)$ denotes the value of surge velocity signal at the n -th moment, $ya(n)$ denotes the value of yaw angle differential signal at the n -th moment, $ltn(n)$ denotes the value of lateral thruster control differential signal at the n -th moment, $mt(n)$ denotes the value of main thruster control differential signal at the n -th moment, $T[sv(n)]$ denotes the value of energy operator signal for surge velocity signal at the n -th moment, $T[ya(n)]$ denotes the value of energy operator signal for yaw angle differential signal at the n -th moment, $T[ltn(n)]$ denotes the value of energy operator signal for lateral thruster control differential signal at the n -th moment, $T[mt(n)]$ denotes the value of energy operator signal for main thruster control differential signal at the n -th moment.

(d) Weak fault feature enhancement based on the MB method

This step is part of the traditional fault feature enhancement method [20], which is briefly described below.

The MB method is used for weak fault feature enhancement to extract the fault feature value.

4. Experiment Verification

The IARO-VMD method is proposed in this study to address the issue of the long-running time of the denoising method based on VMD in reference [20]. The EO-MB method is proposed to tackle the problem of the unsatisfactory enhancement of the weak fault features of the MB. In this section, experiments are conducted to validate these two methods.

In Section 4.1, the experimental environment is briefly introduced. In Section 4.2, the effectiveness of IARO-VMD is verified. In Section 4.3, the effectiveness of EO-MB is verified.

4.1. Experimental Environment

“Beaver II” was directed to track the surge velocity of 0.3 m/s in the experiment. “Beaver II” is shown in Figure 3, and the experimental conditions are shown in Figure 4 [18].

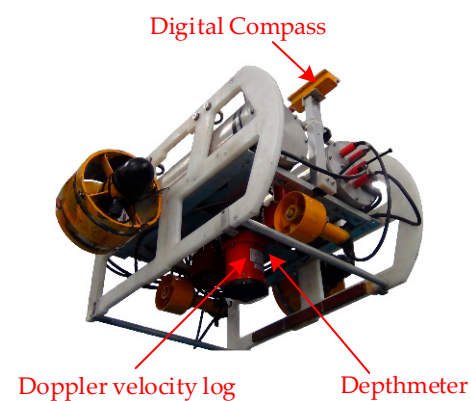


Figure 3. Beaver II AUV experimental prototype.

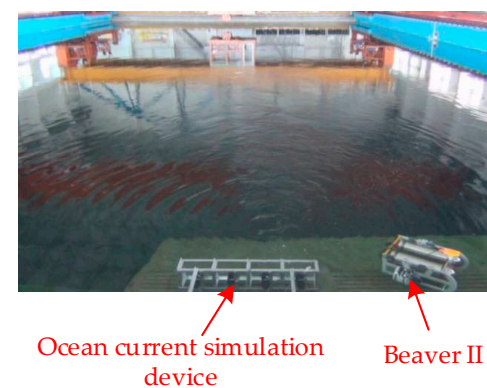


Figure 4. Experimental condition.

In the pool experiment, the target velocity of AUV was 0.3 m/s, and the control period was 0.2 s. The AUV started from a static state and continued to accelerate until it reached the target speed. Then, the AUV operated in a straight line at its target velocity. From the 250th beat, the fault soft simulation method was used to simulate the left main thruster fault until the end of the experiment [18]. Different cases of thruster fault severity were simulated, including 10%, 8%, and 5% thrust loss in one thruster.

4.2. Experiment Verification of IARO-VMD

The noise reduction method based on VMD in reference [20] has a good noise reduction effect, but it is time-consuming. Therefore, in this study, ARO is introduced to reduce the running time. However, after the introduction of ARO, the running time is reduced, but the noise reduction effect is compromised. Consequently, this study proposes IARO-VMD,

which aims to reduce the running time and improve the noise reduction effect simultaneously. Therefore, in this section, the following three methods are compared and experimentally validated: the noise reduction method based on VMD in reference [20], the VMD noise reduction method with the introduction of ARO, and the proposed IARO-VMD method.

In Section 4.2.1, the effectiveness of the proposed IARO-VMD method in noise reduction and running time reduction is verified. In Section 4.2.2, the effects of the two proposed improvements (see Section 2.3) are explained in detail.

4.2.1. Effectiveness of IARO-VMD in Noise Reduction and Running Time Reduction

In this section, comparative experiments were conducted on the noise reduction effects and algorithm running time for fault severities of 10%, 8%, and 5%. The VMD-based method described in reference [20], the VMD-based method with the inclusion of ARO, and the proposed IARO-VMD method were tested in comparison experiments. The above three methods were applied to noise reduction, and a noise reduction effect diagram was obtained. References [28–30] focus on rotating machinery. However, in this study, the diagnosis of the thruster is based on the force generated by propeller rotation in order to propel the AUV forward, which falls outside the scope of rotating machinery. Therefore, the methods proposed in references [28–30] cannot be directly applied to the subject of this study.

We conducted noise reduction experiments on the surge velocity signal, yaw angle signal, lateral thruster control signal, and main thruster control signal. The noise reduction effect taking the surge velocity signal with a fault severity of 10%, as an example, is shown in Figure 5.

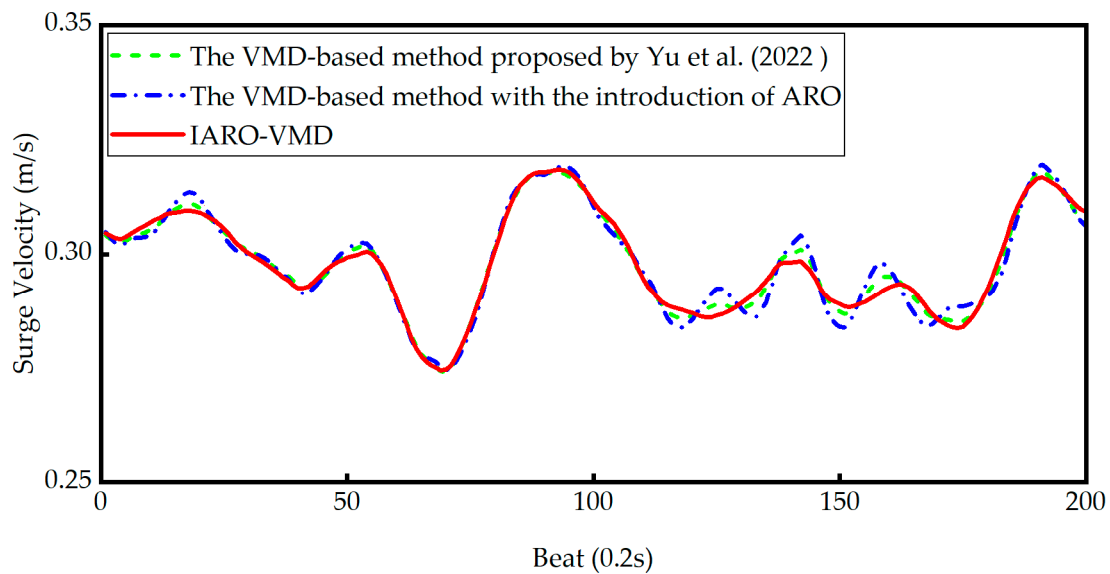


Figure 5. Noise reduction effect of surge velocity signal with 10% fault severity; Yu et al. (2022) [20].

To analyze the problem conveniently, the noise reduction effects and running times of surge velocity signals with all levels of fault severity are summarized in Table 2. The parameter for measuring the noise reduction effect is SNR [40,41]. SNR refers to the ratio between the power of the denoised signal and the power of the noisy signal, which is described as:

$$SNR = \frac{P_{\text{denoised signal}}}{P_{\text{noise signal}}} \tag{9}$$

where $P_{\text{denoised signal}}$ and $P_{\text{noise signal}}$ are the power of the denoised signal and the power of the noise signal, respectively.

Table 2. Comparison of noise reduction effects (SNR) and running times of different methods.

Fault Severity	The VMD-Based Method in Reference [20]		The VMD-Based Method with the Introduction of ARO		IARO-VMD	
	SNR	Running Time (s)	SNR	Running Time (s)	SNR	Running Time (s)
10%	36.18	302.2	37.15	10%	36.18	302.2
8%	36.58	420.3	36.24	8%	36.58	420.3
5%	38.06	395.2	36.14	5%	38.06	395.2

The formula for the power of a signal is as follows:

$$P = \frac{1}{N} \sum_{n=1}^N x(n)^2 \tag{10}$$

where N is the length of the discrete signal $x(n)$.

Next, we will compare and analyze the data presented in Table 2.

(1) Analyze the effectiveness of the VMD-based method with the introduction of ARO.

Firstly, the effect of the VMD-based method in reference [20] is briefly described. The method proposed in reference [20] is to reduce the noise of the AUV thruster fault signal based on VMD. As Table 2 shows, for different degrees of fault severity, the SNR ranges from approximately 36.18 to 38.06. Overall, the noise reduction effect of this method is quite good. However, the running time of this method ranges from 302.2 s to 420.3 s, which is relatively long.

Secondly, the VMD-based method with ARO is analyzed. As shown in Table 2, for different fault severities, the running time is about 34 s, which is about 90% lower than that of the VMD-based method in reference [20]. The running time of the algorithm is affected by the computer hardware used, making the time reduction more meaningful. This reflects the effectiveness of introducing ARO to reduce running time. However, overall, the SNR will be affected by the reduction. For faults with a severity of 8% and 5%, the SNR decreases by about 9.30% and 5.05%, respectively. For faults with a severity of 10%, the SNR slightly increases (2.68%).

(2) Analyze the effectiveness of the IARO-VMD method.

The IARO-VMD method is proposed to solve the problem of SNR reduction in the VMD-based noise reduction method with ARO. As can be seen from Table 2, the SNR of the IARO-VMD method increases significantly. For different levels of faults, it increases by approximately 9.16% to 10.85%, proving that IARO-VMD can effectively improve the noise reduction effect and increase the SNR. In terms of the running time, for different fault severities, the time consumed by IARO-VMD ranges from 32.5 to 36.6 s, and the time consumed using the original ARO method ranges from 33.2 to 35.7 s. The two values are very close to each other, with a small difference. Overall, the proposed IARO-VMD method can effectively improve the noise reduction effect, and the running time is basically the same.

(3) A comparative analysis of effectiveness is conducted between the IARO-VMD- and VMD-based methods in reference [20].

As shown in Table 2, IARO-VMD reduces the running time by approximately 89.25–91.30% and increases the SNR by approximately 5.25–12.27% for different degrees of severity of fault. This proves that IARO-VMD not only solves the problem of excessive running time in the VMD-based method in reference [20] but also significantly improves the SNR.

(4) Comparison of computation load (runtime) of various methods.

Table 2 shows the runtimes of the method proposed in reference [20] (302.2–420.3 s), the VMD denoising method with ARO (32.2–35.7 s), and the VMD denoising method with improved ARO (32.5–36.6 s). When comparing the runtimes, we can make the following observations.

- (1) The running time of the VMD-based method with the introduction of ARO is about 10% of that of the method proposed in reference [20]. This indicates that the introduction of the ARO method can effectively reduce the running time.
- (2) The runtime of IARO-VMD is comparable to that of the VMD-based method with the introduction of ARO, with a negligible difference. This suggests that the improvement of ARO in this study does not introduce a significant increase in the computation load of the ARO algorithm.
- (3) The runtime of IARO-VMD is approximately 10% of that of the method proposed in reference [20]. This indicates that IARO-VMD effectively addresses the issue of the long runtime of the method proposed in reference [20].

Based on the above analysis, it can be concluded that IARO-VMD not only addresses the issue of the long runtime of the method proposed in reference [20], but it also enhances noise reduction.

4.2.2. The Respective Effects of Improvement (1) and Improvement (2)

In Section 2.3, the two improvements of IARO-VMD are outlined. To illustrate the effects of each improvement, this subsection conducts experimental verification.

Improvement (1) and Improvement (2) of IARO-VMD are intended to reduce the noise of surge velocity signals with fault severities of 10%, 8%, and 5%, respectively. Taking the surge velocity signal with 10% fault severity as an example, the noise reduction effects when only using Improvement (1) and when only using Improvement (2) in IARO-VMD are shown in Figure 6.

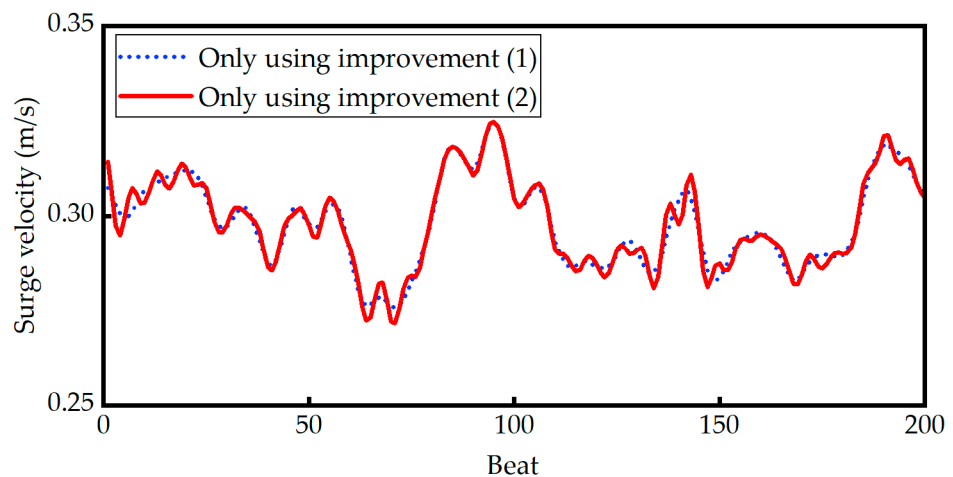


Figure 6. Noise reduction effect of using only Improvement (1) and Improvement (2).

From Figure 6, it can be seen that both Improvement (1) and Improvement (2) achieved good noise reduction effects. Moreover, only using Improvement (1) resulted in smoother curves, larger peaks, and smaller fluctuations, indicating that only using Improvement (1) has a better noise reduction effect. In order to further compare and discuss the respective effects of the two improvements, we have compiled the noise reduction effects (SNR) on all levels of fault severity into Table 3.

Table 3. Summary of the noise reduction effects of using only Improvement (1) and only Improvement (2).

Fault Severity	The VMD-Based Method with the Introduction of ARO	Only Using Improvement (1)	Only Using Improvement (2)	IARO-VMD
10%	37.15	38.22	37.68	43.62
8%	36.24	39.55	39.75	39.56
5%	36.14	35.77	38.85	40.06

An analysis of Table 3 can be undertaken as follows:

Firstly, the effect of only using Improvement (1) is analyzed. Overall, the noise reduction effect when only using Improvement (1) is slightly improved, but the effect is not significant. When the fault severity is 10% and 8%, the SNR increases by 2.88% and 9.13%, respectively. However, when the fault severity is 5%, the SNR decreases by 0.8% and 1.02%.

Secondly, the effect of only using Improvement (2) is analyzed. For any fault severity, the SNR increases by 1.43% to 9.69% when using only Improvement (2), demonstrating the effectiveness of Improvement (2) in improving the noise reduction effect.

Thirdly, a comparative analysis is conducted between the effectiveness of IARO-VMD with Improvement (1) and Improvement (2) and its effectiveness with only Improvement (1). The SNR of IARO-VMD increases by approximately 0.02% to 14.13%, indicating that the noise reduction effect of the proposed IARO-VMD method is superior to that when using only Improvement (1).

Finally, a comparative analysis is conducted between the effectiveness of IARO-VMD with Improvement (1) and Improvement (2) and its effectiveness when using only Improvement (2). Overall, the noise reduction effect of IARO-VMD was found to be better than when using only Improvement (2). When the fault severity was 10% and 5%, the SNR of IARO-VMD increased by approximately 15.76% and 3.15%, respectively, while it remained basically the same (decreased by 0.48%) when the fault severity was 8%.

The above experimental results indicate that both Improvements (1) and (2) have certain effects when used individually. However, when applied together, the proposed IARO-VMD method, composed of Improvement (1) and Improvement (2), achieves better noise reduction and SNR improvement.

4.3. Experimental Verification of EO-MB

To address the problem of the poor enhancement effect of the MB method on weak fault features, the energy operator is introduced. To address the issue of the reduced enhancement effect on the yaw angle, lateral thruster control, and main thruster control signals caused by the introduction of the energy operator, we propose a method called EO-MB in this study. Therefore, in this subsection, comparative experiments are conducted to verify the weak fault feature enhancement effect of this EO-MB method on the surge velocity signal, yaw angle signal, lateral thruster control signal, and main thruster control signal, respectively.

In Section 4.3.1, the weak fault feature enhancement effect of this EO-MB method on the surge velocity signal is verified. In Section 4.3.2, the enhancement effect of this EO-MB method on the yaw angle, lateral thruster control, and main thruster control signals is verified.

4.3.1. Weak Fault Feature Enhancement Effect of Surge Velocity Signal

Comparative experiments are conducted here on the weak fault feature enhancement effects on surge velocity signals with fault severities of 10%, 8%, and 5% when using traditional MB methods and the proposed method. Taking the surge velocity signals with a fault severity of 10% as an example, the weak fault feature enhancement effect is shown in Figure 7.

In Figure 7, the peak value of the proposed method is significantly higher than that of the traditional MB method. This proves that the proposed method has a stronger feature enhancement effect on the surge velocity signal with 10% fault severity than the traditional MB method. In order to further compare and discuss the weak fault feature enhancement effects of the proposed method and the traditional MB method, we have compiled the weak fault feature enhancement effects on surge velocity signals with all degrees of fault severity in Table 4. The parameter for measuring the enhancement effect of weak fault features is the fault feature value. The fault feature value refers to the maximum value of the fault feature signal obtained by MB.

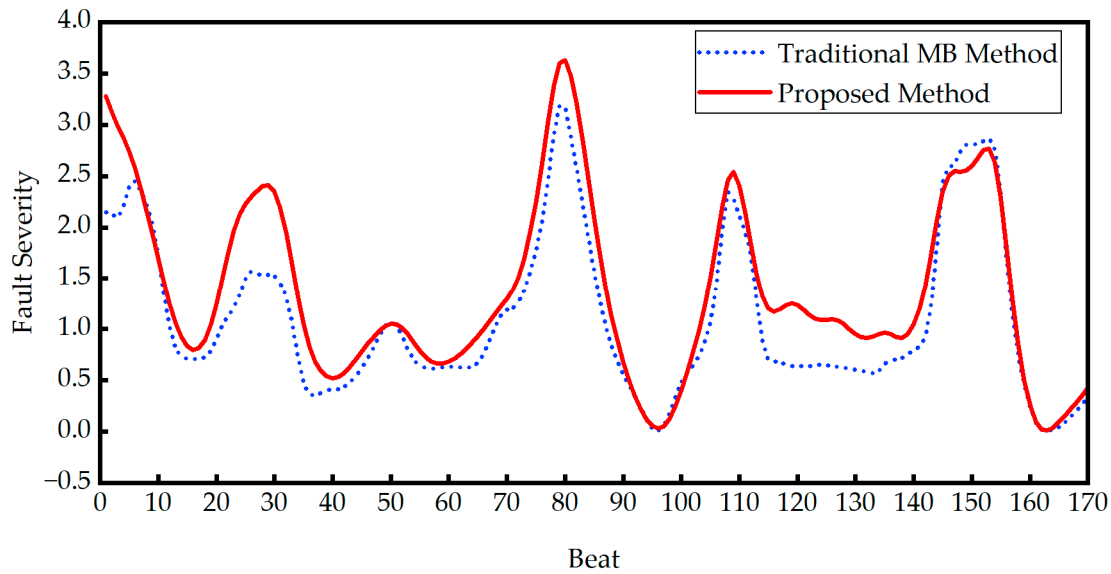


Figure 7. Effect of the weak fault feature enhancement on surge velocity signal with 10% fault severity.

Table 4. Comparison of weak fault feature enhancement effects on surge velocity signals.

Fault Severity	Traditional MB Method		Proposed Method		Percentage of Increase in Fault Feature Value
	Fault Feature Value	Running Time (s)	Fault Feature Value	Running Time (s)	
10%	3.18	32.8	3.63	10%	3.18
8%	2.47	39.8	3.22	8%	2.47
5%	2.66	35.4	2.71	5%	2.66

In Table 4, the percentage of increase in the fault feature value represents the percentage of increase in the fault feature value of EO-MB compared to the fault feature value of the traditional MB method. For example, $14.2\% = (3.63 - 3.18) / 3.18 \times 100\%$.

As shown in Table 4, for the surge velocity signals, the proposed weak fault feature enhancement method is effective for weak faults of any severity, with an increase of 1.9–30.3%. However, for weak faults with a thrust loss of 5%, the fault severity is so low that the enhancement achieved by the proposed method is limited. The running time of this method is between 32.7 s and 39.6 s, and the running time of the IARO-VMD method proposed in Section 2 is between 32.5 and 39.6 s; that is, they are basically the same. In summary, the proposed method improves the effect of fault feature enhancement while maintaining a similar running time.

4.3.2. Weak Fault Feature Enhancement Effect of the Yaw Angle Signal, Lateral Thruster Control Signal, and Main Thruster Control Signal

In this section, comparative experiments were conducted on the weak fault feature enhancement of the yaw angle signal, lateral thruster control signal, and main thruster control signal with fault severities of 10%, 8%, and 5%. The traditional MB method, the method employing the energy operator alone, and the proposed method (adding differential and energy operators) were used for the comparative experiments. Taking the yaw angle signal with a fault severity of 10% as an example, the weak fault feature enhancement effect is shown in Figure 8.

In Figure 8, the peak value of the proposed method is significantly greater than that of the employing energy operator alone and equal to the peak value of the traditional MB method. This indicates that for the yaw angle signal with 10% fault severity, adding the signal differential processing can solve the problem of the fault feature values obtained by employing the energy operator alone being lower than those obtained by the traditional MB

method. In order to further compare and discuss the weak fault feature enhancement effect of the proposed method after adding the differential processing step, we have compiled the weak fault feature enhancement effects on all degrees of fault severity of the yaw angle signal, the main thruster control voltage signal, and the lateral thruster control voltage signal into Tables 5–7, respectively.

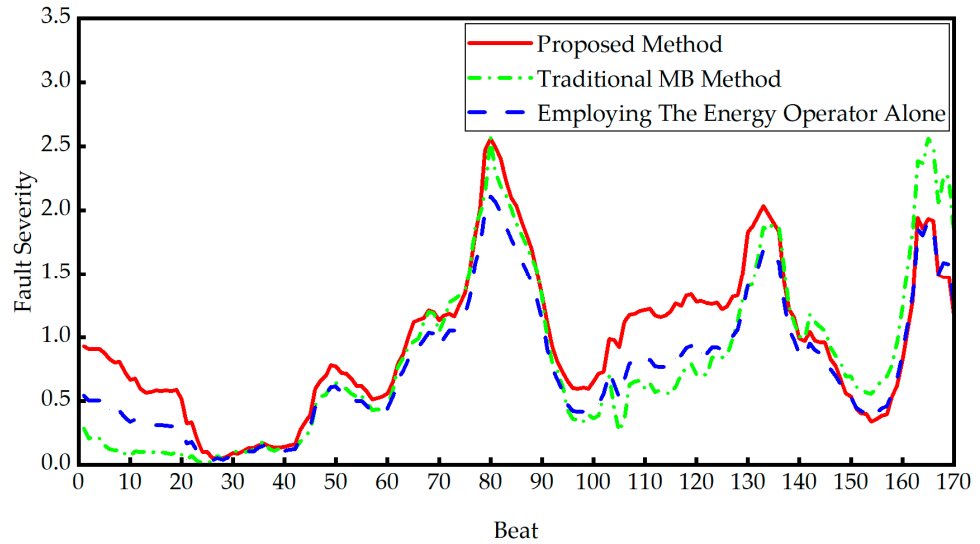


Figure 8. Weak fault feature enhancement effect on yaw angle signal with fault severity of 10%.

Table 5. Comparison of weak fault feature enhancement effect on the yaw angle signal.

Fault Severity	Traditional MB Method		Employing the Energy Operator Alone		Proposed Method		Percentage of Increase in Fault Feature Value
	Fault Feature Value	Running Time (s)	Fault Feature Value	Running Time (s)	Fault Feature Value	Running Time (s)	
10%	2.56	33.1	2.11	33.2	2.56	33.4	0.00%
8%	1.90	40.5	1.56	39.9	2.23	38.3	17.37%
5%	1.65	35.9	1.08	36.3	1.71	36.6	3.64%

Table 6. Comparison of weak fault feature enhancement effect on the lateral thrust control signal.

Fault Severity	Traditional MB Method		Employing the Energy Operator Alone		Proposed Method		Percentage of Increase in Fault Feature Value
	Fault Feature Value	Running Time (s)	Fault Feature Value	Running Time (s)	Fault Feature Value	Running Time (s)	
10%	2.56	35.5	2.14	34.9	2.52	35.9	−1.56%
8%	2.39	38.7	1.37	39.2	3.23	38.2	35.15%
5%	2.15	36.9	2.45	35.6	2.71	36.1	26.05%

Table 7. Comparison of weak fault feature enhancement effect on the main thruster control signal.

Fault Severity	Traditional MB Method		Employing the Energy Operator Alone		Proposed Method		Percentage of Increase in Fault Feature Value
	Fault Feature Value	Running Time (s)	Fault Feature Value	Running Time (s)	Fault Feature Value	Running Time (s)	
10%	3.56	39.8	2.88	39.4	3.62	38.3	1.69%
8%	2.89	37.2	3.26	36.9	3.78	37.3	30.80%
5%	1.78	40.1	2.01	39.5	2.07	38.2	16.30%

Taking the yaw angle signal with a fault severity of 5% as an example, it can be seen from Table 5 that when only the energy operator is added, the fault feature decreases

instead of increasing from 1.65 to 1.08. However, in this study, after signal processing using differential and energy operators, the fault feature increases to 1.71, which is an improvement of 3.6% compared with the traditional MB method. From Tables 6 and 7, it can be seen that the fault features of the main thruster control signal and the lateral thruster control signal are enhanced in the same way as the yaw angle signal, according to the proposed method. The running times of these algorithms are similar to that in Table 4. The experimental results reflect the effectiveness of this method.

5. Conclusions

This study addresses weak fault feature extraction for AUV thrusters. First, we introduce ARO to solve the problem of the long-running time when using the noise reduction method based on VMD in reference [20]. Then, we propose a VMD denoising method based on an improved ARO algorithm, called IARO-VMD, to address the issue of deteriorations in the fault feature extraction effect after introducing ARO. In this method, the chaotic mapping and Gaussian mutation are used to improve ARO and, thus, optimize the parameters of VMD. This leads to a reduced running time and improved fault feature extraction performance. Finally, the pool experiment results of the “Beaver II” AUV prototype show that for weak faults of the AUV thrusters, with thrust losses of 10%, 8%, and 5%, the running time of the proposed IARO-VMD method is reduced by 89.25%, 91.30%, and 91.12%, respectively. At the same time, the fault feature extraction effect is improved by 12.27%, 8.15%, and 5.25%, respectively. The experimental results verify the effectiveness of the IARO-VMD method.

We also studied weak fault feature enhancement for AUV thrusters. After extracting weak fault features of the AUV thruster, it is necessary to enhance the fault features. First, in this study, a weak fault feature enhancement method, called EO-MB, based on energy operators and MB, is proposed to address the issue of the unsatisfactory enhancement effects of the traditional MB method. We then add differential processing to the signal to address the issue of certain fault feature values decreasing after introducing energy operators. Finally, the pool experiment results of the “Beaver II” AUV prototype show that, for weak faults of the AUV thrusters with thrust losses of 10%, 8%, and 5%, compared to the traditional MB method, the proposed EO-MB method imparts the following enhancements:

The surge velocity signal is enhanced by 14.2%, 30.3%, and 1.9%.

The yaw angle signal is enhanced by 0.00%, 17.37%, and 3.64%.

The main thruster voltage signal is enhanced by −1.56%, 35.15%, and 26.05%.

The lateral thruster control signal is enhanced by 1.69%, 30.80%, and 16.30%.

To sum up, the experimental results verify the effectiveness of this method.

Due to factors such as the high complexity of the algorithms, the large data volume required, and the substantial time requirements, the proposed method may induce a significant time lag when used for real-time fault diagnosis. We will continue to try to optimize the implementation of this algorithm so as to reduce the runtime and meet all requirements.

Author Contributions: Conceptualization, D.Y. and M.Z.; methodology, D.Y.; software, D.Y.; validation, D.Y., F.Y., M.Z. and J.L.; formal analysis, D.Y. and M.Z.; investigation, D.Y. and M.Z.; resources, J.L. and M.Z.; data curation, M.Z., F.Y. and J.L.; writing—original draft preparation, D.Y.; writing—review and editing, J.L. and M.Z.; visualization, J.L.; supervision, J.L.; project administration, M.Z.; funding acquisition, M.Z. All authors have read and agreed to the published version of the manuscript.

Funding: This work was supported by the National Natural Science Foundation of China (62303128, 51839004) and the Natural Science Foundation in Heilongjiang Province, China, under Grant YQ2022F003.

Institutional Review Board Statement: Not applicable.

Informed Consent Statement: Not applicable.

Data Availability Statement: The datasets generated during and/or analyzed during the current study are available from the corresponding author upon reasonable request.

Acknowledgments: The authors would like to thank the funder for supporting them and the Editor and Reviewers for their constructive comments.

Conflicts of Interest: The authors declare no conflicts of interest.

References

- Xu, J.; Huang, F.; Wu, D.; Cui, Y.; Yan, Z.; Zhang, K. Deep reinforcement learning based multi-AUVs cooperative decision-making for attack-defense confrontation missions. *Ocean Eng.* **2021**, *239*, 109794. [[CrossRef](#)]
- Zhang, X.; Shan, X.; Xie, T.; Miao, J. A new sensor inspired by the lateral-line system of fish using the self-powered d_{33} mode piezoelectric diaphragm for hydrodynamic sensing. *Mech. Syst. Signal Proc.* **2020**, *141*, 106476. [[CrossRef](#)]
- Fang, X.; Xie, L.H.; Li, X.L. Distributed localization in dynamic networks via complex laplacian. *Automatica* **2023**, *151*, 110915. [[CrossRef](#)]
- Hernandez-Sanchez, A.; Poznyak, A.; Chairez, I.; Andrianova, O. Robust 3-D autonomous navigation of submersible ship using averaged sub-gradient version of integral sliding mode. *Mech. Syst. Signal Proc.* **2021**, *149*, 107169. [[CrossRef](#)]
- Wang, F.R.; Chen, Z.; Song, G.B. Smart crawfish: A concept of underwater multi-bolt looseness identification using entropy-enhanced active sensing and ensemble learning. *Mech. Syst. Signal Proc.* **2021**, *149*, 107186. [[CrossRef](#)]
- Li, J.T.; Wang, Z.H.; Wang, Y.J.; Zhang, M.J.; Raissi, T. Interval Velocity Estimation for Unmanned Underwater Vehicles. *IEEE Control Syst. Lett.* **2023**, *7*, 715–720. [[CrossRef](#)]
- Gao, S.; He, B.; Yu, F.; Zhang, X.; Yan, T.H.; Feng, C. An abnormal motion condition monitoring method based on the dynamic model and complex network for AUV. *Ocean Eng.* **2021**, *237*, 109472. [[CrossRef](#)]
- Che, G.F.; Yu, Z. ADP based output-feedback fault-tolerant tracking control for underactuated AUV with actuators faults. *J. Intell. Fuzzy Syst.* **2023**, *45*, 5871–5883. [[CrossRef](#)]
- Lin, X.; Tian, W.; Zhang, W.; Zeng, J.; Zhang, C. The leaderless multi-AUV system fault-tolerant consensus strategy under heterogeneous communication topology. *Ocean Eng.* **2021**, *237*, 109594. [[CrossRef](#)]
- Zhu, C.; Huang, B.; Zhou, B.; Su, Y.M.; Zhang, E.H. Adaptive model-parameter-free fault-tolerant trajectory tracking control for autonomous underwater vehicles. *Isa Trans.* **2021**, *114*, 57–71. [[CrossRef](#)]
- Wu, P.; Harris, C.A.; Salavasidis, G.; Lorenzo-Lopez, A.; Kamarudzaman, I.; Phillips, A.B.; Thomas, G.; Anderlini, E. Unsupervised anomaly detection for underwater gliders using generative adversarial networks. *Eng. Appl. Artif. Intell.* **2021**, *104*, 104379. [[CrossRef](#)]
- Zhu, D.; Cheng, X.; Yang, L.; Chen, Y.; Yang, S.X. Information Fusion Fault Diagnosis Method for Deep-Sea Human Occupied Vehicle Thruster Based on Deep Belief Network. *IEEE Trans. Cybern.* **2022**, *52*, 9414–9427. [[CrossRef](#)]
- Zhang, M.; Yin, B.; Liu, W.; Wang, Y. Feature extraction and fusion for thruster faults of AUV with random disturbance. *J. Huazhong Univ. Sci. Technol. Nat. Sci. Ed.* **2015**, *43*, 22–26, 54. [[CrossRef](#)]
- Hamilton, K.; Lane, D.M.; Brown, K.E.; Evans, J.; Taylor, N.K. An integrated diagnostic architecture for autonomous underwater vehicles. *J. Field Robot.* **2007**, *24*, 497–526. [[CrossRef](#)]
- Li, J.; Li, J.; Chen, H.; Zhang, Y.; Xie, Y. Propeller feature extraction of UUVs study based on CEEMD combined with symmetric correlation. In Proceedings of the 2nd International Conference on Computer Science Communication and Network Security (CSCNS), Sanya, China, 22–23 December 2021. [[CrossRef](#)]
- Xiang, X.B.; Yu, C.Y.; Zhang, Q. On intelligent risk analysis and critical decision of underwater robotic vehicle. *Ocean Eng.* **2017**, *140*, 453–465. [[CrossRef](#)]
- Shi, H.; Song, Z.; Bai, X.; Zhang, K. Attention mechanism-based multisensor data fusion neural network for fault diagnosis of autonomous underwater vehicles. *J. Field Robot.* **2023**. [[CrossRef](#)]
- Zhang, M.; Yin, B.; Liu, X.; Guo, J. Thruster fault identification method for autonomous underwater vehicle using peak region energy and least square grey relational grade. *Adv. Mech. Eng.* **2015**, *7*, 1687814015622905. [[CrossRef](#)]
- Gong, W.; Lv, T.; Wang, Y.; Di, F. Weak Fault Feature Extraction Method for Autonomous Underwater Vehicles based on Wavelet Packets and FFT. In Proceedings of the 4th IEEE Advanced Information Technology, Electronic and Automation Control Conference, IAEAC 2019, Chengdu, China, 20–22 December 2019. [[CrossRef](#)]
- Yu, D.; Zhang, M.; Liu, X.; Yao, F. Fault feature extraction and fusion method for AUV with weak thruster fault based on variational mode decomposition and D-S evidence theory. *Math. Biosci. Eng.* **2022**, *19*, 9335–9356. [[CrossRef](#)]
- Cui, D.; Zhang, T.; Zhang, M.; Liu, X. Feature extraction and severity identification for autonomous underwater vehicle with weak thruster fault. *J. Mar. Sci. Technol.* **2022**, *27*, 1105–1115. [[CrossRef](#)]
- Dragomiretskiy, K.; Zosso, D. Variational Mode Decomposition. *IEEE Trans. Signal Process.* **2014**, *62*, 531–544. [[CrossRef](#)]
- Li, J.; Chen, Y.; Qian, Z.H.; Lu, C.G. Research on VMD based adaptive denoising method applied to water supply pipeline leakage location. *Measurement* **2020**, *151*, 107153. [[CrossRef](#)]
- Cui, H.; Guan, Y.; Chen, H. Rolling Element Fault Diagnosis Based on VMD and Sensitivity MCKD. *IEEE Access* **2021**, *9*, 120297–120308. [[CrossRef](#)]

25. Jin, Z.; Chen, D.; He, D.; Sun, Y.; Yin, X. Bearing Fault Diagnosis Based on VMD and Improved CNN. *J. Fail. Anal. Prev.* **2023**, *23*, 165–175. [[CrossRef](#)]
26. Jiang, X.; Shen, C.; Shi, J.; Zhu, Z. Initial center frequency-guided VMD for fault diagnosis of rotating machines. *J. Sound Vib.* **2018**, *435*, 36–55. [[CrossRef](#)]
27. Yan, X.A.; Jia, M.P. Application of CSA-VMD and optimal scale morphological slice bispectrum in enhancing outer race fault detection of rolling element bearings. *Mech. Syst. Signal Proc.* **2019**, *122*, 56–86. [[CrossRef](#)]
28. Wu, L.; Liu, Y.; Wu, S.; Ren, J.; Teng, W. Composite fault diagnosis of wind turbine gearboxes based on VMD cepstral transform. *J. Vib. Shock* **2023**, *42*, 221–256. [[CrossRef](#)]
29. Feng, R.; Yinzhong, Y.; Xianghua, M. Application of VMD-AR method in fault diagnosis of ROV propeller. In Proceedings of the 11th CAA Symposium on Fault Detection, Supervision, and Safety for Technical Processes, SAFEPROCESS 2019, Xiamen, China, 5–7 July 2019. [[CrossRef](#)]
30. Zhao, Y.J.; Li, C.S.; Fu, W.L.; Liu, J.; Yu, T.; Chen, H. A modified variational mode decomposition method based on envelope nesting and multi-criteria evaluation. *J. Sound Vib.* **2020**, *468*, 115099. [[CrossRef](#)]
31. Wang, L.; Cao, Q.; Zhang, Z.; Mirjalili, S.; Zhao, W. Artificial rabbits optimization: A new bio-inspired meta-heuristic algorithm for solving engineering optimization problems. *Eng. Appl. Artif. Intell.* **2022**, *114*, 105082. [[CrossRef](#)]
32. Vellingiri, M.; Rawa, M.; Alghamdi, S.; Alhussainy, A.A.; Ali, Z.M.; Turkey, R.A.; Refaat, M.M.; Aleem, S. Maximum hosting capacity estimation for renewables in power grids considering energy storage and transmission lines expansion using hybrid sine cosine artificial rabbits algorithm. *Ain Shams Eng. J.* **2023**, *14*, 102092. [[CrossRef](#)]
33. Li, Y.J.; Wang, J.X.; Feng, D.J.; Jiang, M.S.; Peng, C.; Geng, X.Y.; Zhang, F.Y. Bearing fault diagnosis method based on maximum noise ratio kurtosis product deconvolution with noise conditions. *Measurement* **2023**, *221*, 113542. [[CrossRef](#)]
34. Zhang, R.C.; Sun, W.L.; Liang, W.Z. Kernel principal component analysis fault diagnosis method based on improving Golden Jackal optimization algorithm. *Proc. Inst. Mech. Eng. Part I-J. Syst. Control Eng.* **2023**. [[CrossRef](#)]
35. Chen, Y.G.; Wang, Q.S.; Zhong, R.; Shi, X.J.; Qin, B. Fiber orientation and boundary stiffness optimization of laminated cylindrical shells with elastic boundary for maximum the fundamental frequency by an improved sparrow search algorithm. *Thin-Walled Struct.* **2023**, *193*, 111299. [[CrossRef](#)]
36. Wang, X.; Xu, D. A novel image encryption scheme based on Brownian motion and PWLCM chaotic system. *Nonlinear Dyn.* **2014**, *75*, 345–353. [[CrossRef](#)]
37. Nezhad, S.Y.D.; Safdarian, N.; Zadeh, S.A.H. New method for fingerprint images encryption using DNA sequence and chaotic tent map. *Optik* **2020**, *224*, 165661. [[CrossRef](#)]
38. Xu, Y.; Wang, Y.; Wang, L.; Qu, J. Bearing fault detection using an alternative analytic energy operator: A fast and non-filtering method. *Meas. Sci. Technol.* **2021**, *32*, 105101. [[CrossRef](#)]
39. Wang, Y.; Gu, L.; Xu, Y. Enhancement of bearing fault detection using an alternative analytic energy operator and sparse Bayesian step-filtering. *J. Mech. Sci. Technol.* **2021**, *35*, 905–920. [[CrossRef](#)]
40. Xu, H.; Cai, C.; Chi, Y.; Zhang, N. Fault diagnosis of gearbox based on adaptive wavelet de-noising and convolution neural network. *Adv. Mech. Eng.* **2023**, *15*, 16878132231157186. [[CrossRef](#)]
41. Wang, X.; Zhang, H.; Du, Z. Multiscale Noise Reduction Attention Network for Aeroengine Bearing Fault Diagnosis. *IEEE Trans. Instrum. Meas.* **2023**, *72*, 3513810. [[CrossRef](#)]

Disclaimer/Publisher’s Note: The statements, opinions and data contained in all publications are solely those of the individual author(s) and contributor(s) and not of MDPI and/or the editor(s). MDPI and/or the editor(s) disclaim responsibility for any injury to people or property resulting from any ideas, methods, instructions or products referred to in the content.